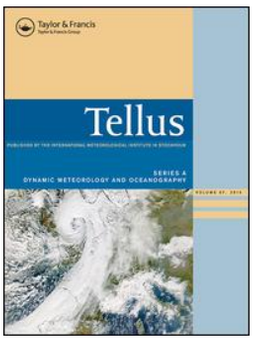

Tellus A: Dynamic Meteorology and Oceanography

ISSN: (Print) 1600-0870 (Online) Journal homepage: https://www.tandfonline.com/loi/zela20

The North Atlantic Oscillation signal in a regional climate simulation for the European region

Roxana Bojariu & Filippo Giorgi

To cite this article: Roxana Bojariu & Filippo Giorgi (2005) The North Atlantic Oscillation signal in a regional climate simulation for the European region, Tellus A: Dynamic Meteorology and Oceanography, 57:4, 641-653, DOI: 10.3402/tellusa.v57i4.14709

To link to this article: https://doi.org/10.3402/tellusa.v57i4.14709

Tellus (2005), 57A, 641–653
Printed in Singapore. All rights reserved

TELLUS

The North Atlantic Oscillation signal in a regional climate simulation for the European region

By ROXANA BOJARIU[1]* and FILIPPO GIORGI[2], [1]*Administratia Naţionala de Meteorologie, Sos. Bucuresti-Ploiesti 97, 013686, Bucharest, Romania;* [2]*Abdus Salam International Centre for Theoretical Physics (ICTP), Trieste, Italy*

(Manuscript received 7 April 2004; in final form 29 November 2004)

ABSTRACT

The North Atlantic Oscillation (NAO) is a dominant pattern of large-scale variability in the Northern Hemisphere, with important regional effects on the winter climate of Europe. Nested regional climate models (RCMs) can be useful tools for studying the regional signal of the NAO. Therefore, it is important to assess whether they can reproduce the observed NAO signal over Europe when driven by lateral boundary conditions from global climate models. In this paper we investigate the NAO-related winter variability over Europe in a RCM simulation driven by large-scale fields from an atmospheric global model simulation forced with historic sea surface temperature and sea ice distribution for the period 1961–1990. We show that (1) the NAO-related winter variability signal over the European region shows substantial topographically induced fine-scale features, both for temperature and precipitation, and (2) the model is capable of reproducing many aspects of this fine-scale regional signal and, in particular, the topographically forced regional response of precipitation to NAO-type circulations. We conclude that nested regional climate models can be used to study the fine-scale regional signature of the NAO under different climatic conditions.

1. Introduction

The North Atlantic Oscillation (NAO) is an important component of the variability of the Northern Hemisphere winter climate (e.g. Rodwell et al., 1999; Bojariu and Gimeno, 2003). The NAO is defined in the sea level pressure (SLP) anomaly field as a dipole-like structure characterized during the positive phase by a strong Icelandic low and Azores high (e.g. Van Loon and Rogers, 1978). Over land, positive NAO phase conditions lead to negative surface air temperature anomalies over western Greenland and northeastern Canada, and positive temperature anomalies over central and northern Europe. In winter, dry conditions over southern Europe and the Mediterranean area, and positive precipitation anomalies from Iceland to Scandinavia, are also associated with the positive NAO phase (e.g. Hurrell, 1995). Opposite conditions are found during the negative NAO phase. Over the ocean, the two NAO phases determine opposite changes in the North Atlantic westerlies and trades, the position and intensity of the storm track, the heat and fresh water flux and the pattern of sea surface temperature (SST) anomalies (Cayan, 1992; Rogers, 1997; Bojariu and Reverdin, 2002).

*Corresponding author.
e-mail: bojariu@meteo.inmh.ro

The large-scale features of the influence of the NAO on the European winter climate are well known (e.g. Hurrell, 1995). However, the fine-scale characteristics of the NAO signal have been analysed less extensively. The strength of the NAO signal is highly variable within the European region due to local factors. Hanssen-Bauer and Førland (2000) found that the effect of the NAO on the long-term trends and decadal scale variability of temperature and precipitation in Norway is locally modulated, with the southwestern part of the country being most affected. A pronounced spatial variability of the NAO signal over northern Europe was also found by Uvo (2003).

A number of studies identified spatially variable responses of Iberian precipitation to the NAO. These responses range from a high sensitivity in the central and southwestern regions of the peninsula to low sensitivity in the southeastern regions due to the influence of topography and the Mediterranean Sea (Rodo et al., 1997; Esteban-Parra et al., 1998; Rodríguez-Puebla et al., 1998; Martin-Vide and Gomez, 1999; Ulbrich et al., 1999; Sáenz et al., 2001; Goodess and Jones, 2002; Muñoz-Díaz and Rodrigo, 2003). Schmidli et al. (2002) found that the correlation between precipitation and the NAO index (NAOI) is negative and relatively stationary south of the main Alpine crest, while it is highly intermittent north of the crest. Finally, Bojariu and Paliu (2001) identified a strong influence of the Carpathian mountains on the NAO-related temperature and

precipitation anomalies in Romania for the period 1961–1990. Thus, the observational evidence suggests that topography and land–sea contrasts add fine-scale detail to the NAO-related large-scale temperature and precipitation signal over the European region.

Regional climate models (RCMs) can be very valuable tools for studying the fine-scale signal of the NAO because they can reach horizontal resolutions of a few tenths of a kilometre. In particular, the use of RCMs driven by lateral boundary conditions from global model simulations can allow us to study how the regional effects of the NAO can change under the forcing of increased greenhouse gas concentrations. Indeed, during the last decade, RCMs have been increasingly used for simulations of regional climates under a variety of boundary conditions and forcing scenarios (e.g. McGregor, 1997; Giorgi and Mearns, 1991, 1999), and a number of nested RCM simulations have been carried out over Europe (e.g. Giorgi and Marinucci, 1996; Giorgi et al., 1997; Jones et al., 1995, 1997; Christensen et al., 1997, 1998; Rotach et al., 1997; Machenhauer et al., 1998; Räisänen et al., 2001; Räisänen and Joelsson 2001; Jacob et al., 2001; Räisänen et al., 2004; Giorgi et al., 2004). However, to date no investigation has been presented of the fine-scale NAO signal in RCM simulations.

To fill this gap, we present an analysis of the NAO signature in a multidecadal simulation over Europe with a RCM driven by lateral forcing fields from a corresponding experiment with an atmospheric general circulation model (AGCM). The simulation, which was completed under the European project PRUDENCE (Prediction of Regional scenarios and Uncertainties for defining EuropeaN Climate change risks and Effects; Christensen et al., 2002), covers the period 1961–1990, during which the NAO showed a multidecadal trend towards an increasingly positive phase (Hurrell, 1995).

Our analysis is aimed at assessing whether the nested modelling system captures the winter NAO variability signal over Europe and its modulation by regional topographical features. Large-scale NAO signals are essentially imposed by the large-scale AGCM fields used to drive the RCM simulation, while fine-scale signals are due to the internal RCM processes and forcings (e.g. topography). A good overall simulation of the NAO variability thus requires a good performance by both the global model, which provides the lateral boundary conditions for the RCM, and the RCM itself. In this paper we analyse the NAO signal in the RCM simulation and compare it with that of the driving AGCM in order to assess the influence of the large-scale AGCM forcing fields on the local topographical NAO-related features. This comparison can also provide an illustration of the added fine-scale information that can be obtained when using a nested RCM to downscale AGCM information. This paper focuses on the NAO-related spatial patterns rather than their predictability, and this constitutes the first step towards the assessment of regional NAO-induced signals under various climate change scenarios.

We first perform an analysis of the NAO-related patterns for the entire European domain, with emphasis on some key regions where the NAO signal is strongly modulated by the local topography, such as Scandinavia, the Balkan/Alpine region and the Iberian Peninsula. As a more detailed illustrative example, we then focus on a relatively small region encompassing the Carpathian mountain chain and adjacent areas for which we have available accurate observations from a relatively large number of observing stations (104).

2. Model, data, experiment design and methodology of analysis

2.1. Model, data and simulation

The simulation analysed in the present study is described in detail by Giorgi et al. (2004). It was completed using the regional model RegCM in the version originally developed by Giorgi et al. (1993a,b) and later improved as described by Giorgi and Mearns (1999) and Pal et al. (2000). The model horizontal grid interval is 50 km and the domain covers most of Europe and the Mediterranean Basin (Fig. 1) using a Lambert conformal projection. The RegCM was run at its standard configuration, with the model top at 80 hPa, 14 vertical sigma layers and five levels below about 1.5 km.

The driving lateral boundary conditions for the RegCM simulation are obtained from a corresponding experiment with the Hadley Centre's HadAM3H AGCM (Pope et al., 2000), which uses a horizontal grid point spacing of 1.25° latitude and 1.875° longitude. The lateral boundary conditions are provided using the modified relaxation procedure of Giorgi et al. (1993b) and the RegCM is run continuously for the entire 1961–1990 period. The HadAM3H simulation uses observed monthly SST, sea ice,

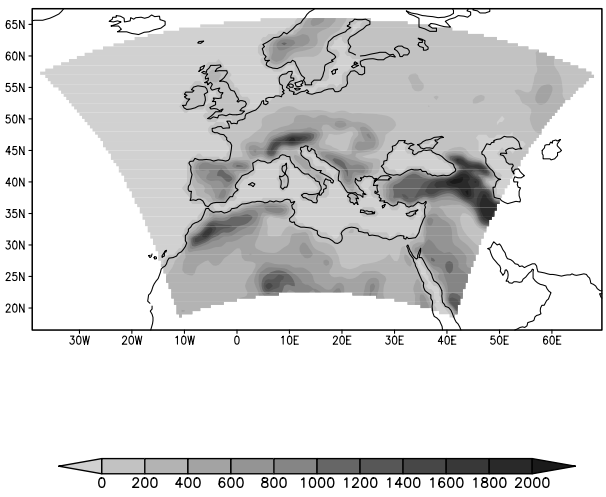

Fig. 1. RegCM domain and topography. The map projection is Lambert conformal. Units are m.

greenhouse gas (GHG) and sulfur emissions. From the sulfur emissions, HadAM3H calculates sulfate aerosol concentrations using an atmospheric sulfur model. SST, sea ice, GHG and sulfate concentrations are then interpolated onto the RegCM grid and used by the regional model to calculate the corresponding radiative forcing, including both direct and indirect aerosol effects (Giorgi et al., 2002, 2003). A brief summary of the salient features of the 1961–1990 RegCM experiment is reported in Section 3.1 and for more details the reader is referred to Giorgi et al. (2004).

Since the effects of the NAO are most important during the winter season, in this study we focus on winter climate as defined by the period December–January–February (DJF). The observed data used to evaluate the model simulation are taken from the monthly data set developed at the Climatic Research Unit (CRU) of the University of East Anglia (New et al., 2000). This is a station-based 0.5° resolution gridded dataset of surface air temperature and precipitation over land for the period 1901–2001, out of which we extracted data for 1961–1990. The resolution of the CRU data is thus similar to that of the RegCM. For the more detailed analysis of the Carpathian region we use observations of winter temperature and precipitation from 104 Romanian stations for the period 1962–1990. Monthly SLP from the NCEP/NCAR reanalysis (Kalnay et al., 1996) are also used to evaluate the model experiment. As a measure of the observed NAO intensity we use the station-based DJF NAOI provided by the Climate Analysis Section, NCAR, Boulder, CO, USA, defined as the difference between the normalized SLP at Ponta Delgada, Azores, and Stykkisholmur/Reykjavik, Iceland (Hurrell, 1995).

2.2. *Analysis methodology*

We use a multivariate statistical method, the canonical correlation analysis (CCA), to identify the NAO-related variability. The CCA selects a pair of spatial patterns of two variables such that their time evolutions are optimally correlated (Preisendorfer, 1988; Bretherton et al., 1992; Von Storch, 1995). Prior to performing the CCA, the data are projected onto their empirical orthogonal functions (EOFs) and only a limited number of EOFs are retained in order to minimize noise. Typically, the canonical correlation tends to be overestimated if the number of EOFs is too large and a compromise needs to be achieved between the requirement of having a high fraction of the total variance captured in the set of CCA patterns and the constraint to filter out noise from the data (Von Storch, 1995).

We apply the CCA to the pairs of variables SLP/temperature and SLP/precipitation for both modelled and observed data. In the EOF analysis we use the covariance matrix of the data. The EOF and CCA patterns are normalized such that the temporal coefficients are in standard deviation units. We compare the CCA time evolution of temperature and precipitation with each other and with the NAOI.

The use of non-standardized anomalies as input for the EOF analysis and subsequent CCA (i.e. the use of the covariance matrix) presents the advantage of a good representation of gradients in the analysed fields, and thus facilitates the physical interpretation of the results. However, some regional features tend to be masked due to the contrast between different climate characteristics coexisting in the analysis area. For this reason we perform a parallel analysis by mapping the correlation coefficients between the principal component associated with the first EOF of SLP over Europe (as a measure of the NAOI) and the temperature or precipitation at each grid point (or station). Linear regression and non-parametric Mann–Kendall rank statistics (τ) (Sneyers, 1990) are used to detect trends in both modelled and observed data.

3. Results

3.1. *Brief description of the 1961–1990 RegCM simulation*

As mentioned, the RegCM simulation analysed here has been described in detail by Giorgi et al. (2004) and only a brief summary of their main conclusions is given here. Overall, the RegCM captured well both the spatial patterns and seasonal evolution of the large-scale average wind field, surface air temperature and precipitation. Seasonally averaged temperature biases were mostly less than 1–2 °C. The model showed a tendency to overestimate precipitation, particularly in the spring season. However, the precipitation biases (10–20%) were mostly within the estimated uncertainties in the observational data sets.

Giorgi et al. (2004) also examined the simulated interannual variability of temperature and precipitation over different European areas and found that the RegCM underestimated the temperature variability in winter over central and eastern Europe while it reproduced well the observed winter variability over the Mediterranean region. Summer temperature variability was instead generally overestimated. Concerning precipitation, the variability was well reproduced over western, central and eastern Europe, while it was overestimated over the Mediterranean Basin in summer.

Finally, an analysis of the simulated trends during the period 1961–1990 showed that, despite the availability of a single simulation, the model was successful in reproducing some patterns of observed trends, especially for precipitation. In particular, the model reproduced the observed winter drying trend over the Mediterranean area and the increasing winter precipitation trend over continental Europe. The large-scale features of the RegCM and HadAM3H simulations were generally similar because of the strong influence of the forcing HadAM3H fields on the regional model. Significant differences were, however, found at the finer scales, either in response to local topographic and coastline forcings or because of the representation of local physical processes.

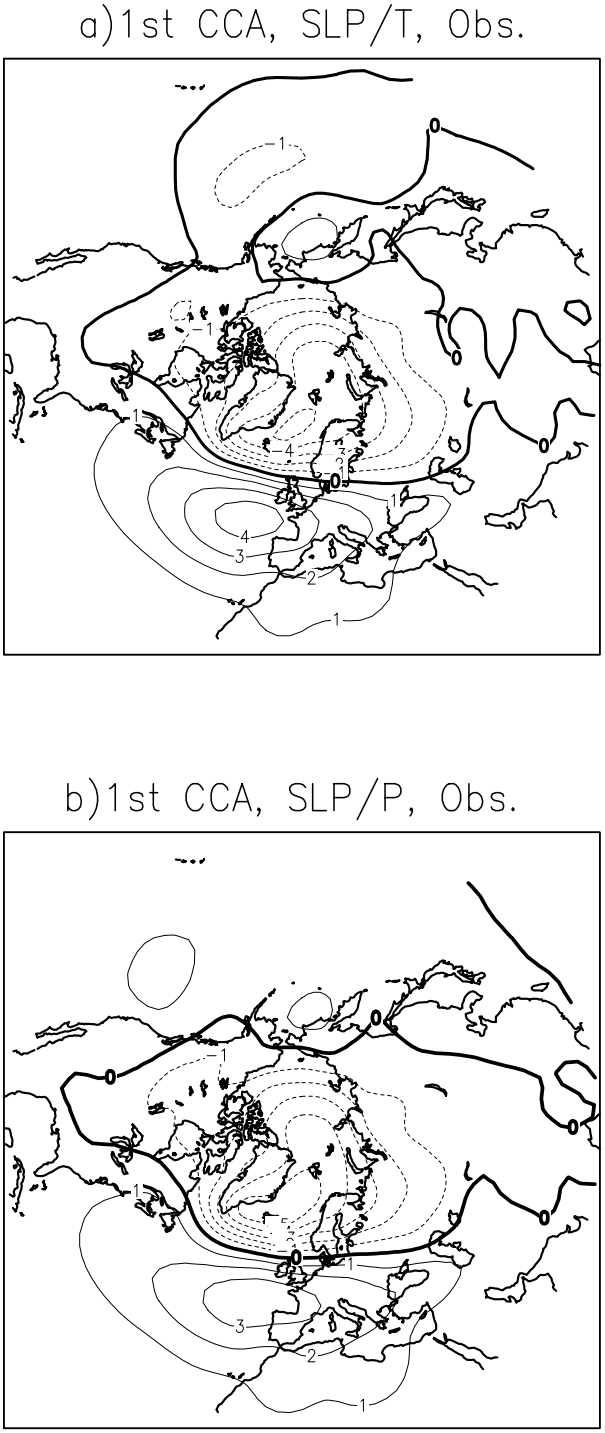

Fig. 2. Observed spatial pattern of leading CCA modes for the pairs DJF SLP/temperature (a) and DJF SLP/precipitation (b) for the period 1961–1990. Units are hPa. The winter (DJF) SLP is from the NCEP/NCAR reanalysis, while temperature and precipitation are from the CRU dataset.

3.2. The observed winter NAO-related variability signal over Europe during 1961–1990

We identify the NAO-related patterns in observed temperature and precipitation over Europe by performing the CCA on the CRU gridded data and the NCAR/NCEP Northern Hemisphere SLP (north of 20°N) for the winters (DJF) of 1961–1990. Figures 2a and b illustrate the leading CCA spatial patterns of SLP paired with averaged temperature and precipitation anomalies, respectively. Tests with different numbers of EOFs suggested that the best choice in terms of both highest correlation and explained variance is to retain the first five EOFs of SLP, precipitation and temperature. For the SLP/temperature pair, the correlation coefficient associated with the first CCA mode is 0.93 and the fraction of total variance represented is 0.40 for SLP and 0.38 for temperature. For the SLP/precipitation pair, the correlation coefficient associated with the first CCA mode is also 0.93 and the fraction of total variance represented is 0.42 for SLP and 0.26 for precipitation. The time evolution of the CCA modes is significantly correlated with the NAOI for the analysed period, with correlation coefficients of 0.88 and 0.81 for the SLP/precipitation and the SLP/temperature pairs, respectively (Fig. 3a). The spatial patterns of the observed first CCA mode over Europe are shown in Fig. 4a for the SLP/temperature pair and in Fig. 5a for the SLP/precipitation pair. The CRU temperature and precipitation data are interpolated onto the RegCM grid and do not include ocean values.

The patterns displayed in Figs. 2, 4a and 5a are consistent with the large-scale features of winter NAO variability revealed by other studies (e.g. Van Loon and Rogers, 1978; Hurrell, 1995). During the positive NAO phase, enhanced westerly circulation prevails, bringing warm air from the North Atlantic to northern and central Europe. Also, the Atlantic storm track is displaced northwards from its average position and the baroclinic activity over the Mediterranean Sea is strongly inhibited due to a reduction of the north–south thermal gradient. This causes the observed negative precipitation anomalies over southern Europe.

Opposite conditions are found during the negative NAO phase, when enhanced northeasterly wind anomalies prevail over northern and central Europe and induce negative surface air temperature anomalies there. The Atlantic storm track is then displaced southwards of its average position and the advection of moist air over the Iberian Peninsula as well as the baroclinic activity over the Mediterranean area are enhanced. This causes the observed tendency for above normal precipitation over southern Europe during negative NAO phases (e.g. Lamb and Pepler, 1987; Hurrell, 1995; Ulbrich et al., 1999; Sáenz et al., 2001). The effect of the displacement of the Atlantic storm track between the two NAO phases (Rogers, 1997) is clearly revealed in the observations by a dipole structure in the precipitation field, with the peak amplitudes located over southern Scandinavia and the Iberian Peninsula (Fig. 5a).

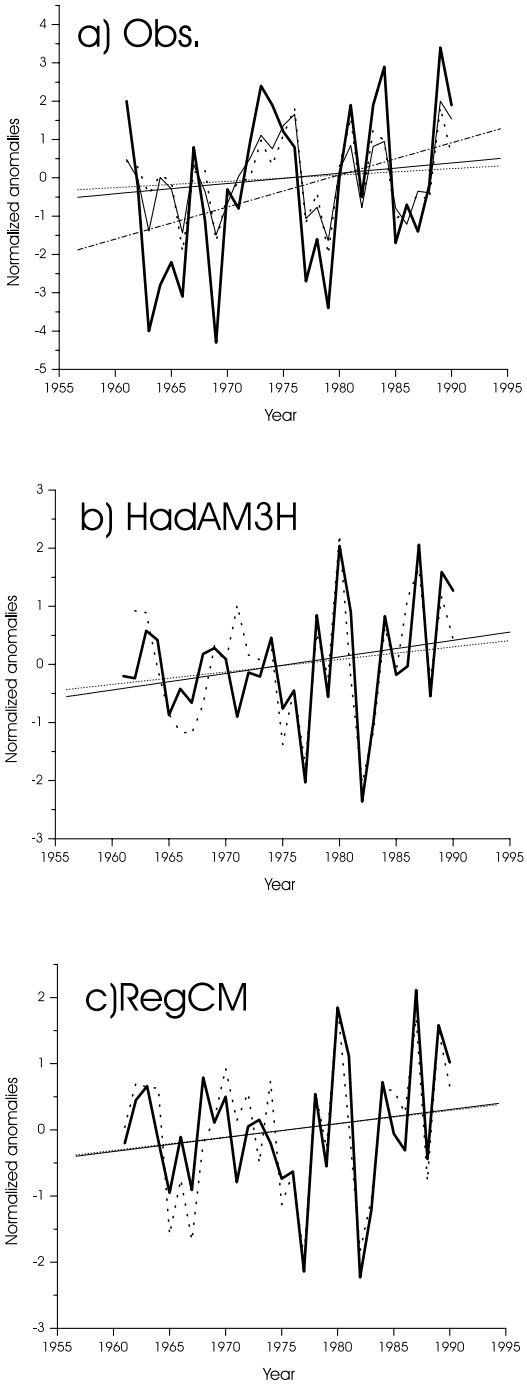

Fig. 3. (a) Time evolution of the NAOI (solid bold curve), the leading observed DJF SLP/temperature CCA mode (solid curve) and the leading observed SLP/precipitation CCA mode (dotted bold curve) of Figs. 2a and b, respectively. (b) DJF RegCM time-series of the leading SLP/temperature (solid bold curve) and SLP/precipitation (dotted bold curve) first CCA modes. (c) DJF HadAM3H time-series of the leading SLP/temperature (solid bold curve) and SLP/precipitation (dotted bold curve) first CCA modes. Also shown are the corresponding linear regression trend lines (dashed-dotted for NAOI, solid thin for temperature and dotted thin for precipitation).

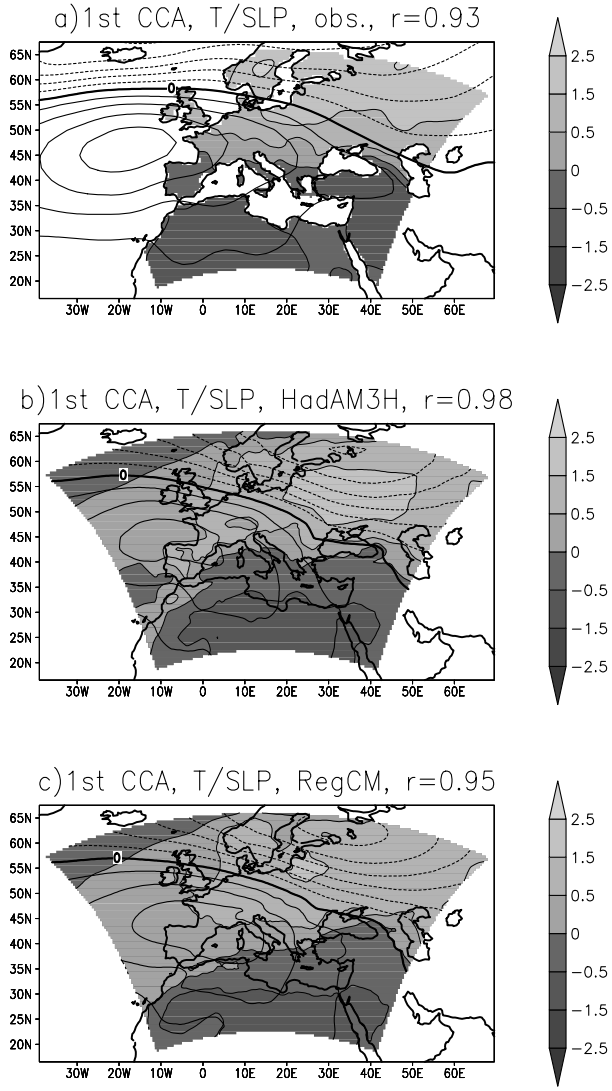

Fig. 4. Spatial pattern of the first CCA mode of DJF SLP (contoured, hPa) and temperature (shaded, °C) representing the observed (a) and the simulated NAO-related variability by the HadAM3H (b) and RegCM (c) over Europe for the period 1961–1990. The SLP contour interval is 1 hPa and solid (dotted) contours are used for the positive (negative) SLP. Zero lines are bold. The observed SLP pattern is the regional portion of the hemispheric patterns in Fig. 2.

In terms of the NAO–precipitation relationship, the spatial structure revealed by the CRU gridded data is generally in agreement with other analyses performed with raw data from meteorological stations. For example, using EOF and cluster analysis applied to data from 125 northern European meteorological stations for the period 1967–1996, Uvo (2003) identified basically the same NAO-related features in the local precipitation field over northern Europe as found in the CCA spatial pattern of Fig. 5a. A strong precipitation variability centre is located over the southwestern Norwegian coast due to the enhancement of

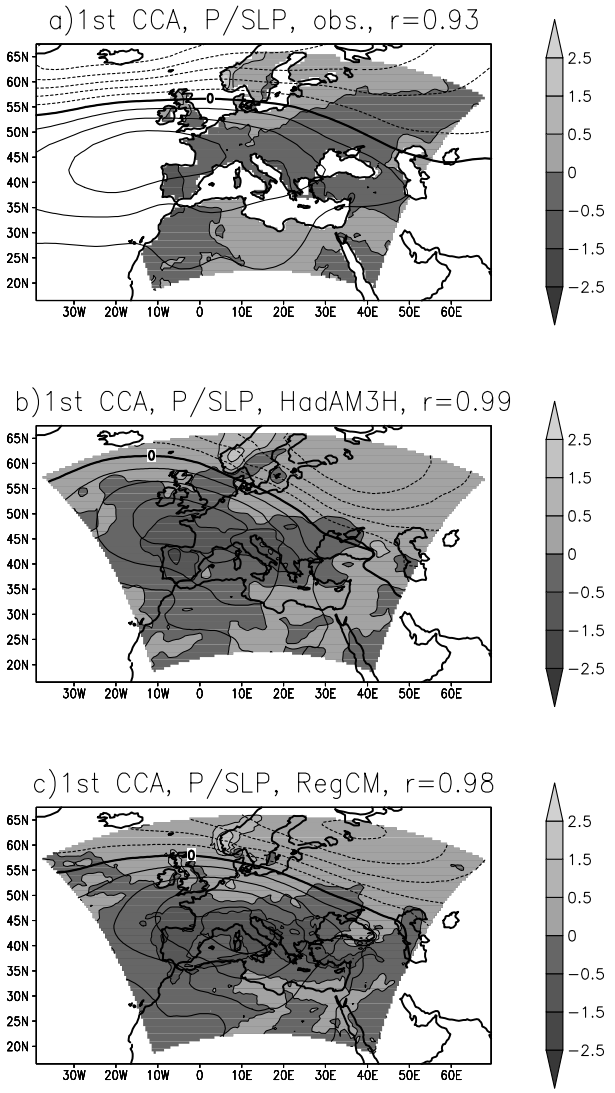

Fig. 5. Spatial patterns of the first CCA mode of DJF SLP (contoured, hPa) and precipitation (shaded, mm/day) representing the observed (a) and simulated NAO-related variability by the HadAM3H (b) and RegCM (c) over Europe for the period 1961–1990. The SLP contour interval is 1 hPa and solid (dotted) contours are used for the positive (negative) SLP. Zero lines are bold. The CRU SLP pattern is the regional portion of the hemispheric patterns in Fig. 2.

precipitation by orographic uplift of moist westerly flow during the positive NAO phase. Less precipitation variability of opposite sign is identified over southeastern Sweden due to the precipitation shadowing effect of the Scandinavian mountains, which presents a barrier to the influence of the NAO, and to the exposure of this area to southeasterly winds from the Baltic Sea.

Another important centre of variability is the Iberian Peninsula, where the NAO signal is strongly affected by the precipitation shadowing effect of the topographic massifs of the Iberian Plateau. This is illustrated by the spatial pattern of the first CCA mode of Fig. 5a and is in agreement with an analysis of Iberian precipitation performed by Rodríguez-Puebla et al. (2001) using data from 56 meteorological stations (see their Fig. 1). Additional topographically modulated variability centres are found along the western coasts of the Balkan Peninsula and Turkey (see Fig. 5a).

The CCA patterns are based on EOFs, which themselves are derived from the covariance matrix of the underlying data. They represent gradients accurately but tend to obscure features present in regions characterized by relatively smaller climate fluctuations. Correlation maps between the principal component associated with the first EOF of SLP over Europe and the CRU grid point temperature and precipitation have been computed to obtain a clearer signal in regions characterized by smaller climate fluctuations. The first EOF of the NCEP/NCAR SLP over Europe is quite similar to the CCA patterns presented in Fig. 2 and it represents 50% of the total variance in the SLP field. Its correlation coefficient with the NAOI is 0.87. Observed correlations for three key centres of variability characterized by pronounced spatial gradients (northern Europe, the Iberian Peninsula and the central Mediterranean) are shown in Figs. 6a, 7a and 8a.

For northern Europe (Fig. 6a), the correlation map clearly shows the effect of regional topography on the NAO patterns, which induces positive correlations over the western Norwegian coasts. For the Iberian Peninsula (Fig. 7a) the correlation map shows that even though most of the area is significantly influenced by the NAO, the strength of the influence of the NAO is greater over the central and southwestern regions (Rodo et al., 1997; Goodess and Jones, 2002). This feature is masked in the CCA pattern (Fig. 5a) due to the low level of rainfall variability in this region.

Over the central Mediterranean (Fig. 8a) we can observe a sharp variation in correlation across the Alpine chain and over the Balkan region. The prevailing negative correlation between the NAO and precipitation over this region is also supported by the analysis of station data of Tomozeiu et al. (2002). They attribute the downward trend in winter precipitation over the Italian Peninsula observed in recent decades to the influence of the NAO.

3.3. The NAO variability signal over Europe in the RegCM and HADAMH3 simulations

We use the same analysis as in Section 3.2 to identify the NAO signal in the 30 yr RegCM experiment, and for comparison purposes the HADAM3H corresponding fields used to drive the regional model. The first five EOFs of SLP, precipitation and temperature are retained in all cases for the subsequent CCA. The NAO-related first CCA mode of the SLP/temperature pair derived from HadAM3H has a correlation coefficient of 0.98 and a fractional total represented variance of 0.54 for SLP and 0.36 for temperature. The HADAM3H NAO-related first CCA mode of the SLP/precipitation pair has a correlation coefficient of 0.99

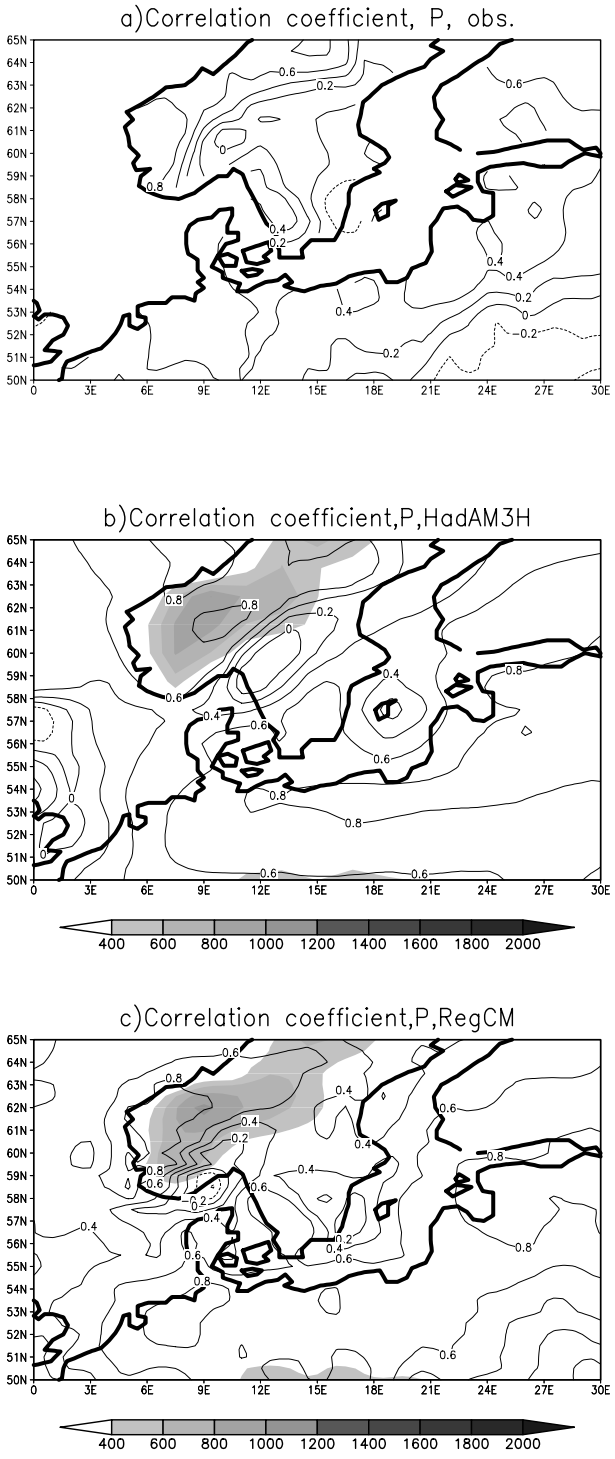

Fig. 6. Correlation coefficient between the first principal component of the DJF SLP and precipitation at each grid point of the northern European region included in our model domain: (a) observations (CRU), (b) HadAM3H simulation, (c) RegCM simulation. Statistically significant coefficients at the 0.95 confidence level are greater than 0.39 in magnitude. Shading indicates HadAM3H topography in (b) and RegCM topography in (c) (units of m).

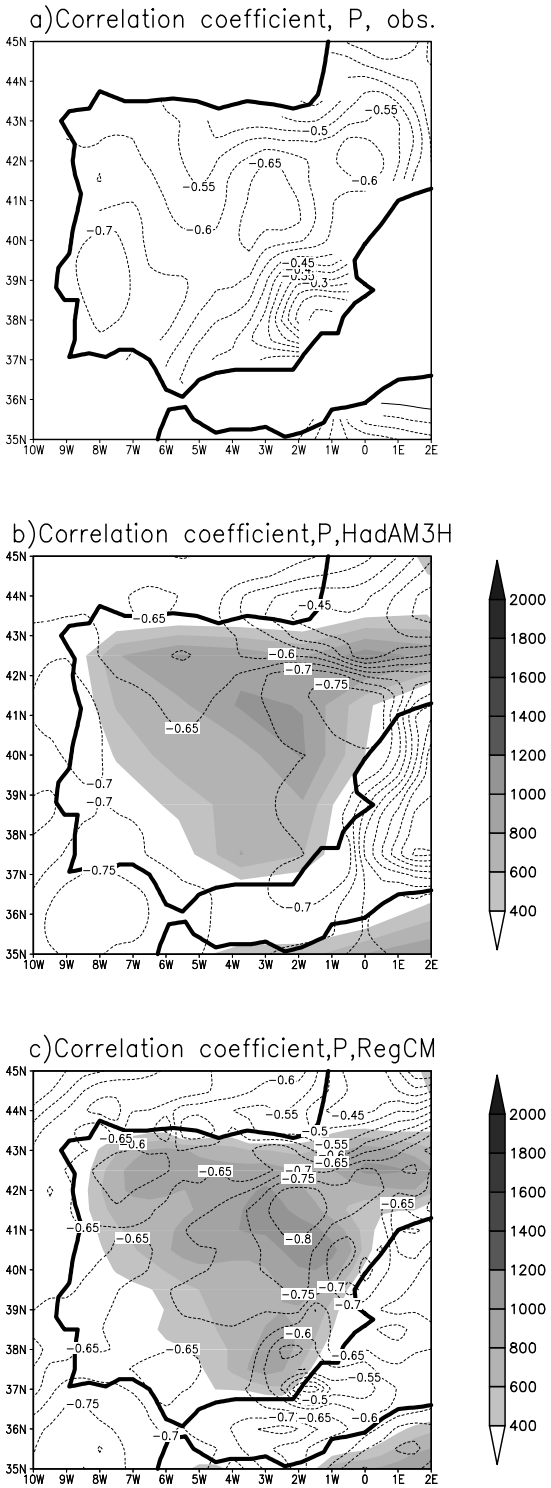

Fig. 7. Correlation coefficient between the first principal component of the DJF SLP and precipitation at each grid point of the Iberian Peninsula: (a) observations (CRU), (b) HadAM3H simulation, (c) RegCM simulation. Statistically significant coefficients at the 0.95 confidence level are smaller than −0.39. Shading indicates HadAM3H topography in (b) and RegCM topography in (c) (units of m).

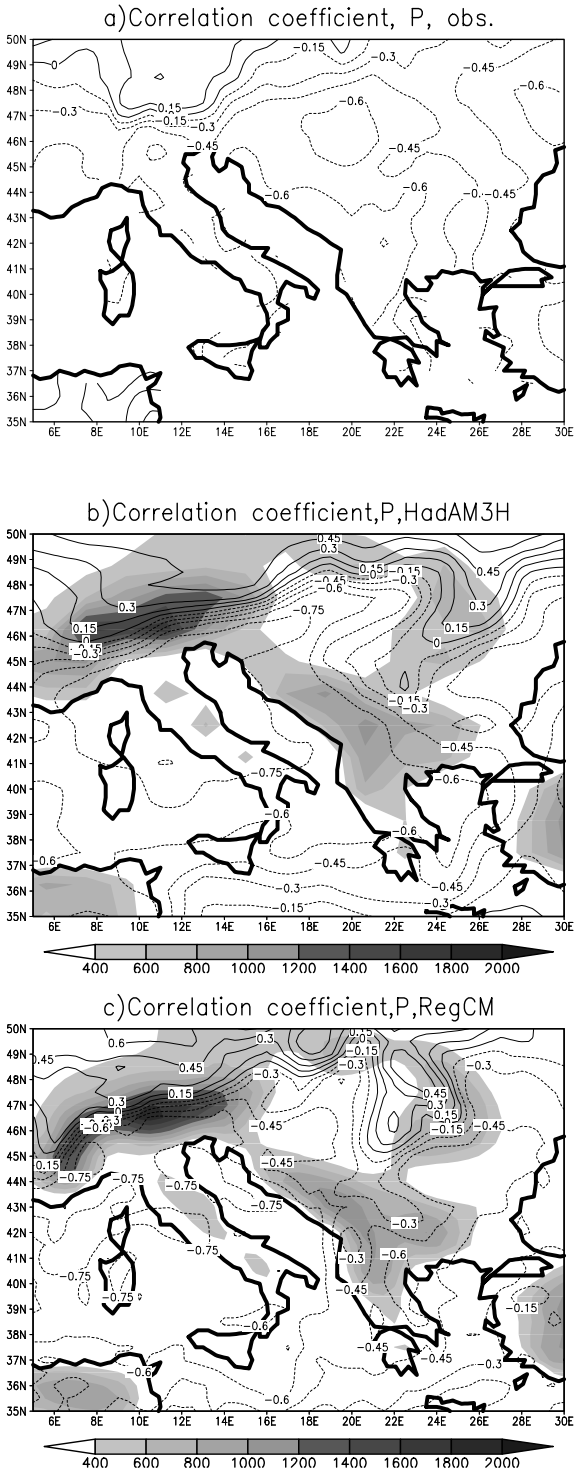

Fig. 8. Correlation coefficient between the first principal component of the DJF SLP and precipitation at each grid point of the central Mediterranean region: (a) observations, (b) HadAM3H simulation, (c) RegCM simulation. Statistically significant coefficients at the 0.95 confidence level are greater than 0.39 in magnitude. Shading indicates HadAM3H topography in (b) and RegCM topography in (c) (units of m).

and a fractional represented variance of 0.38 for SLP and 0.27 for precipitation. For the RegCM SLP/temperature pair the correlation coefficient associated with the first CCA mode is 0.95 and the fraction of total variance represented is 0.50 for SLP and 0.32 for temperature. The RegCM SLP/precipitation pair has a correlation coefficient associated with the first CCA mode of 0.98 and a fraction of total variance represented of 0.43 for SLP and 0.31 for precipitation.

The spatial patterns of the first CCA temperature and precipitation modes in the RegCM and HadAM3H are compared with observations in Figs. 4 and 5. The first EOF of the RegCM SLP (not shown) is quite similar to the CCA SLP pattern presented in Fig. 4b and represents 50% of the total variance in the modelled SLP field. The correlation coefficients of its principal component with the RegCM CCA time series are 0.94 and 0.82 for the temperature-paired and precipitation-paired patterns, respectively. In agreement with observations, the simulated large-scale coupled SLP patterns display a zonal circulation with northern and southern Europe characterized by an out-of-phase relationship. However, the simulated dipole centres are shifted eastwards compared with their observed position in both the HadAM3H and RegCM simulations. As mentioned, the simulation of these large-scale centres of variability is primarily determined by the large-scale forcing fields of HadAM3H (Figs. 4b and 5b).

The spatial features of the simulated regional temperature responses to the NAO-type circulation show some differences compared with observations in both the HADAM3H and RegCM simulations. In the model-derived temperature CCA patterns (Figs. 4b and c) the simulated Scandinavian centre of variability is reduced compared with observations. This feature is due to a shift in the position of the northern centre of action in the driving AGCM fields compared with observations. The magnitude of negative thermal coefficients over Greece, Turkey and the eastern Mediterranean is underestimated by the models.

For precipitation, the amplitude of the first CCA mode is overestimated over southern and central Europe in both models (Figs. 5b and c) but the details of the NAO-related variability are reproduced remarkably well by the RegCM experiment in the regions where the response to the NAO is modulated by the topography and land–sea contrast, in particular over southern Scandinavia, the western Iberian Peninsula and the Balkan Peninsula. The HadAM3H precipitation patterns show a shift relative to the coast in all these key regions. Furthermore, an artificial shadowing effect is apparent in the HadAM3H precipitation pattern over the central portion of southern Scandinavia which is not found in the observations. Finally, the intensification of precipitation variability over the western Turkish coast, which is present in the CRU and RegCM data, is absent in the HadAM3H pattern. All these features are due to the relatively coarse representation of topography in HADAM3H and we conclude that the RegCM simulation is able to better represent the topographically forced details of NAO-related precipitation variability.

Figure 6 compares observed and simulated correlation maps of the first principal component of SLP and precipitation over northern Europe. The combined effect of the Scandinavian mountains and the easterly circulation from the Baltic region is well simulated by the RegCM model, with the correlation strength showing a maximum over the western Norwegian coasts and a minimum over the southeastern regions of Sweden (the shadowing effect). In addition, both the RegCM and CRU data exhibit an area of significant NAO-related precipitation variability over the southwestern Swedish coast (Fig. 6). This feature was also found by Uvo (2003) from station observations. The HADAM3H shifts the western Norwegian maximum to the east and does not simulate the southeastern Swedish maximum.

The local details of NAO-related Iberian precipitation are also generally reproduced by the RegCM in both the covariance based CCA (Fig. 5) and the correlation map (Fig. 7), although the correlation coefficients are generally higher in the model than in the observations. The strongest linkage between precipitation and the NAO is in the central, northeastern and southwestern portions of the Iberian Peninsula, and the RegCM captures this linkage. In addition, in both the RegCM and the observations the correlation decreases over the southeastern and Cantabrian coasts. Using observed data, Sáenz et al. (2001) showed that during the positive NAO phase the main mode of precipitation variability is associated with a strong reduction of baroclinic activity in the baroclinic waveguide which joins the eastern branch of the Atlantic storm track and the Mediterranean Basin. During the negative NAO phase, the increase in baroclinic activity is not significant, suggesting a non-linear behaviour of the precipitation response to the large-scale circulations over the southeastern coasts. Muñoz-Díaz and Rodrigo (2003) explain this behaviour in terms of the increasing influence of the Mediterranean Sea from west to east and of the topographic barrier of the Sierra Nevada mountains. The decrease in correlation strength over the southeastern Iberian coast (as a results of the shadowing effect of the Sierra Nevada mountains) which is present in both the CRU (Fig. 7a) and RegCM (Fig. 7c) patterns is absent in the HadAM3H data (Fig. 7b). The HadAM3H also does not capture the maximum negative correlation over central Spain. Again, similarly to the case for the Scandinavian region, the RegCM performs better than its corresponding AGCM in capturing the topographically induced detail of precipitation variability over the Iberian Peninsula.

Over the central Mediterranean region (Fig. 8) both the global and regional models capture the change in the correlation sign across the Alpine crest, which was also found by Schmidli et al. (2002). Over the Italian and Balkan peninsulas the models and the observations show a prevalence of negative correlations, although in the CRU observations these extend further north over the Balkan region than in the simulations. The topographic signal of the coastal Balkan mountains is especially evident in the RegCM results.

Although the time evolution of the NAO-related signals is not the main concern here, we briefly analyse some temporal trends of the coefficients of the CCA modes, which can be viewed as alternative regional NAO indices. These are shown in Fig. 3 for the SLP/temperature and SLP/precipitation pairs. The linear regression between the NAOI and the time-series associated with the CRU and simulated CCA modes (Fig. 3) suggests the existence of an upward trend in both observed and modelled indices. In addition, the τ values of the Mann–Kendall test (Table 1) computed for the observed and simulated time-series show positive values in all cases (although with a low significance level), implying the presence of upward trends in the data. The model simulations capture the observed trend in the CCA modes, albeit the magnitude of the trends is underestimated. The simulated trend is mostly determined by the NAO-related features from the AGCM transmitted to the RCM and this result suggests that the SST forcing in the driving AGCM may be an important factor in determining the trend. However, a more robust conclusion on the issue of simulated trends in NAO-related patterns would require ensembles of simulations.

3.4. The local NAO variability signal over the Carpathian region

In this section we analyse in more detail the model performance in capturing the local NAO-related signature over Romania using observed data at 104 Romanian stations for the period 1962–1990. Figures 9 and 10 show the first observed and simulated CCA modes in the RegCM and HadAM3H models for the SLP/temperature and SLP/precipitation pairs, respectively. In all cases presented in this paragraph, temperature and precipitation are extracted for a domain covering Romanian territory (from 20°E to 30°E and from 43°N to 49°N). The local spatial coefficients derived from the 104 stations were interpolated onto

Table 1. Mann–Kendall τ statistics for the NAOI and the time series of: the first principal component of the DJF NCEP/NCAR SLP over Europe and the observed DJF (CRU) CCA SLP/temperature and SLP/precipitation pairs; the time-series of the first principal component of simulated DJF SLP over Europe and the CCA DJF SLP/temperature and DJF SLP/precipitation pairs. The bold value are significant at the 95% confidence level and the italic value significant at the 90% confidence level

NAOI	NCEP/NCAR EOF SLP	CRU CCA SLP/T	CRU CCA SLP/P	HadAM3H EOF SLP	HadAM3H CCA SLP/T	HadAM3H CCA SLP/P	RegCM EOF SLP	RegCM CCA T/SLP	RegCM CCA P/SLP
1.72	**2.00**	1.09	0.53	0.96	1.07	0.88	1.03	0.96	0.70

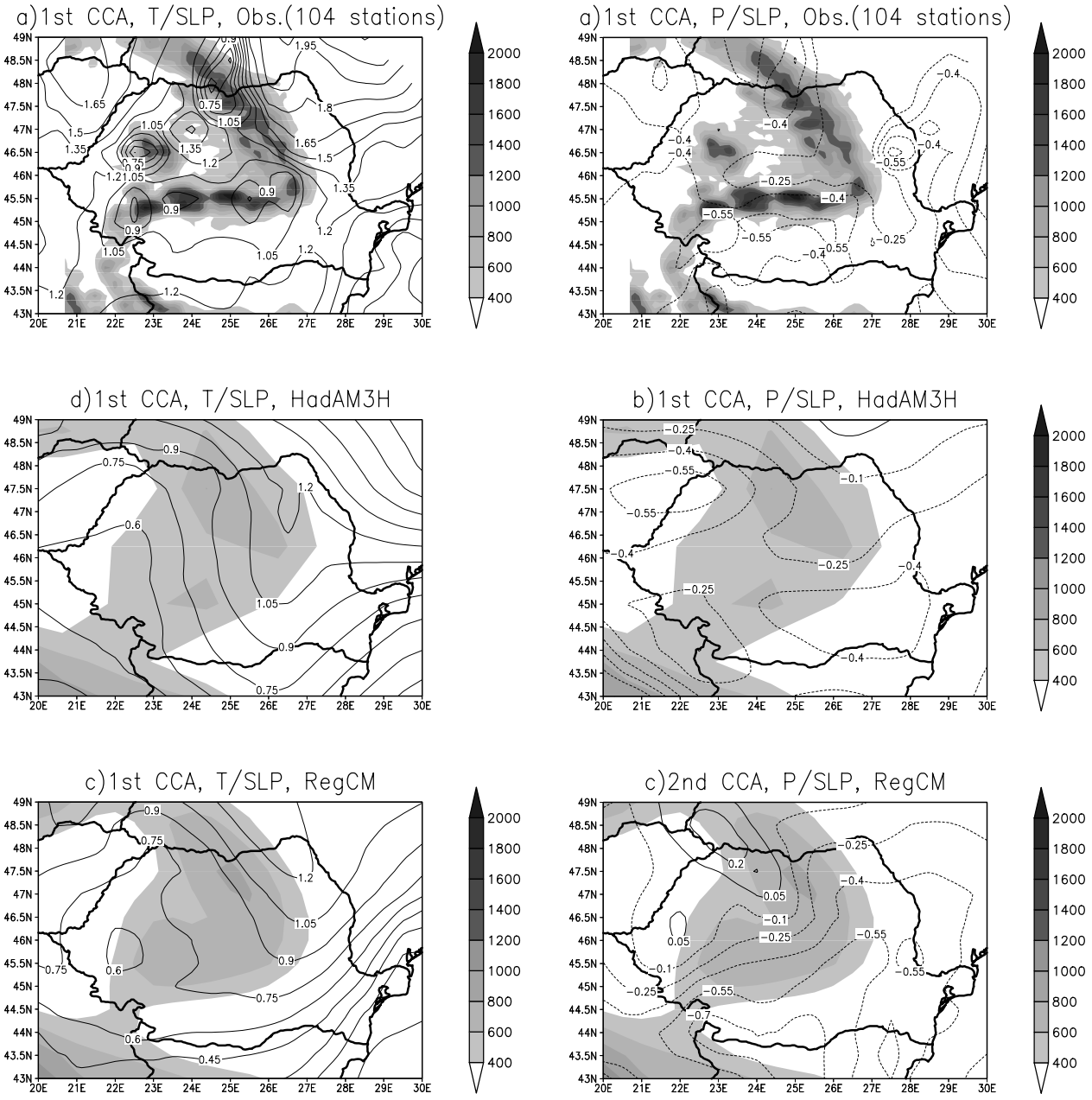

Fig. 9. Spatial pattern of the first CCA mode of the DJF SLP/temperature pair for the interval 1962–1990 derived from (a) 104 Romanian meteorological stations (interpolated onto a 0.5° grid), (b) the HadAM3H simulation and (c) the RegCM simulation. Shading indicates topography (m) from a 10″ resolution data (a) and in the HadAM3H (b) and RegCM (c) models.

Fig. 10. The same as in Fig. 9 but for precipitation.

a 0.5° longitude–latitude grid by applying a Cressman procedure. Note that the observing stations only cover Romanian territory and features outside the Romanian borders are due to the spatial interpolation.

The CCA spatial patterns of hemispheric SLP linked to observed Romanian temperature and precipitation (not shown) are similar to the NCEP/NCAR-derived ones (Fig. 2), displaying an NAO-related dipole structure. Their time-series are statistically correlated with the NAOI for the analysed interval (0.75 and 0.76 for temperature and precipitation, respectively). The correlation coefficient associated with the SLP/temperature and SLP/precipitation CCA pairs is 0.89 and 0.88, respectively. The fraction of total variance represented is 0.24 (0.32) for the SLP paired with temperature (precipitation) and 0.47 (0.35) for temperature (precipitation) paired with the SLP.

A dominant feature of the central and eastern European region, where Romania is located, is the presence of the Carpathian chain, which stretches between 45°N and 50°N and encloses the Hungarian Plain and the Somes-Transylvanian Plateau (see Figs. 8, 9 and 10). Comparison of the RegCM topography maps of Figs. 9c and 10c with the finer-scale topographic data of Figs. 9a and 10a shows that the model captures the general shape of the Carpathian chain, although the chain itself is smoother than in reality and some local topographical features are not represented. The improvement in the topographical representation of the Carpathians between the RegCM and HADAM3H models is also evident from Figs. 9b,c and 10b,c.

The Carpathians represent a strong element of roughness for the atmospheric flow, and the uplift across the Carpathian slopes substantially modulates the precipitation patterns over the region (Ion-Bordei, 1988). The winter NAO-related signal in the temperature field is stronger in the extra-Carpathian regions due to the topographic forcing imposed on the atmospheric flow by the Carpathian mountains (Ion-Bordei, 1988; Bojariu and Paliu, 2001). This signal mainly manifests itself in an intensification of the NAO-related variability to the east and west of the Carpathian Massif, with the eastern centre being more intense due to the greater roughness of the eastern Carpathians (Fig. 9a). Another maximum centre is located in the northwestern portions of the intra-Carpathian region. The main minima in the first temperature CCA mode are found over the branches of the Carpathian chain (Fig. 9a).

The observed winter pattern of precipitation anomalies reveals a strong NAO signal over the southwestern and southern areas of Romania due to an enhanced (decreased) frequency of Mediterranean cyclones reaching this region during negative (positive) NAO phases. A second centre of variability is located over eastern Romania (east of the Carpathians) due to cyclones following a trajectory over, and being intensified by, the Black Sea (Fig. 10a).

The comparison between simulations and observations shows that the RegCM model reproduces a number of features of the response of both the temperature (Fig. 9) and precipitation (Fig. 10) to the NAO large-scale winter variability over Romanian territory. The eastern Romania temperature/SLP pattern is reasonably well reproduced by the RegCM model (see Fig. 9), along with some elements of the thermal structure over the southern regions of Romania. These patterns are less effectively simulated by HadAM3H. RegCM also captures the blocking effect of the Carpathian chain over the western regions of Romania, which is instead lost by HadAM3H (Fig. 9b). The simulated signal over the western slopes of the Carpathians is, however, underestimated by both models. The winter CCA pattern for the RegCM-simulated precipitation anomalies (Fig. 10c) presents a north–south gradient with a maximum located south of the Carpathian chain. This feature is in agreement with observations (Fig. 10a). It is noteworthy that the second centre of precipitation variability located east of the Carpathians and due to the influence of the Black Sea is also captured by the regional model. Neither of these features is present in the HadAM3H patterns. The agreement between simulated and observed CCA precipitation patterns decreases in the northern regions of Romania, probably because of the smoothed model topography.

In summary, even the relatively smooth model representation of the Carpathian chain allows the RegCM model to capture some important aspects of the regional signature of the NAO over Romania. A finer-scale representation of the Carpathian chain would probably lead to a better simulation of the local details associated with the variability of the NAO.

4. Summary and conclusions

In this paper we analyse the winter NAO signal in a nested regional climate simulation over Europe for the period 1961–1990. The phenomenon-oriented approach used here to validate the model results ensures that both the variable climatic features and the underlying physical mechanisms are correctly represented by the model. First, an analysis of observations shows that the NAO signature on the winter temperature and precipitation variability exhibits substantial topographically induced fine-scale detail, particularly over Scandinavia, the Iberian Peninsula and the central Mediterranean. Overall, the RegCM simulation showed a good performance in capturing the main regional features of the European winter climate response to the NAO variability, both in its large-scale and fine-scale features. The large-scale response is primarily determined by the driving global model fields while the fine-scale response is mostly modulated by the regional model topography. As a result, because of its finer topographical representation, the RegCM performs better than the forcing HadAM3H in describing the topographically induced signal of the NAO-related variability. In general, the RegCM shows a better performance in simulating the NAO signal for precipitation than for temperature. One of the reasons for this is that the topographic forcing is a dominant feature affecting winter precipitation, and this forcing is well simulated by the RegCM.

In agreement with observations, upward trends have been found in all simulated NAO indices. This provides some support to the hypothesis that the SST forcing in the AGCM experiment may play a role in the decadal NAO variability simulated by the driving model and transmitted to the RegCM model (Rodwell et al., 1999). However, a more robust conclusion on this issue requires ensembles of simulations. The consistency of the NAO-related trends in the HadAM3H and RegCM time-series also indicates that the temporal variability simulated by the AGCM is correctly downscaled by the regional model. In addition, the agreement between a number of RegCM and observed fine-scale features of the NAO precipitation signal over the Iberian, Scandinavian, Alpine, Balkan and Carpathian regions demonstrates the important role played by the topographic forcing in modulating the large-scale NAO variability over Europe.

Our results suggest that the interaction of large-scale NAO-type circulations with topography is generally more important for precipitation than for temperature. Moreover, our analysis shows that despite the chain of uncertainties from the driving ACGM fields to the nested regional model, RCM simulations are capable of capturing both the broad and fine-scale regional features of variability associated with a non-stationary phenomenon like the NAO. It is important to stress that because the large-scale signal is essentially dominated by the forcing AGCM fields and the smaller-scale signal is dominated by the RCM description of local forcings (e.g. topography and coastlines), the successful simulation of NAO-related effects requires a good performance in both the driving global model and the nested regional model.

Pozo-Vázquez et al. (2001) studied the linearity of local climate responses to the NAO in observed data over Europe and found that the NAO–climate relationship is not stationary in time. Non-stationarity was also found by Solonosky et al. (2001) in a study of circulation and temperature data over Europe from the 1770s to 1995. These results suggest that the extrapolation of current NAO–temperature linkages to future climate conditions should be taken very cautiously.

As a preferred internal mode of the extratropical atmosphere, the NAO will evolve in a changing climate system, possibly leading to non-stationary changes in its regional and local responses. As a result, nested RCMs can be especially useful tools (e.g. compared with statistical downscaling) to study small-scale responses to the NAO-related variability under changing forcing conditions (e.g. greenhouse gas concentration).

5. Acknowledgments

This work was supported by the European Union Programme Energy, Environment and Sustainable Development under contract EVK2-2001-0056 (PRUDENCE). We would like to thank two anonymous reviewers for their useful comments, which helped to improve the quality of this paper.

References

Bojariu, R. and Gimeno, L. 2003. Predictability and numerical modelling of the North Atlantic Oscillation. *Earth Sci. Rev.* **63**(1–2), 145–168.

Bojariu, R. and Paliu, D. 2001. North Atlantic Oscillation projection on Romanian climate fluctuations in the cold season. In: *Detecting and Modelling Regional Climate Change and Associated Impacts* (eds M. Brunet and D. Lopez). Springer, Berlin, 345–356.

Bojariu, R. and Reverdin, G. 2002. Large-scale variability modes of freshwater flux and precipitation over the Atlantic. *Clim. Dynam.* **18**, 369–381.

Bretherton, C. S., Smith, C. and Wallace, J. M. 1992. An intercomparison methods for finding coupled patterns in climate data. *J. Climate* **5**, 541–560.

Cayan, D. R. 1992. Latent and sensible heat flux anomalies over the northern oceans: the connection to monthly atmospheric circulation. *J. Climate* **5**, 354–369.

Christensen, J. H., Carter, T. R. and Giorgi, F. 2002. PRUDENCE employs new methods to assess European climate change. *EOS, Trans. Am. Geophys. Un.* **83**(13), 26.

Christensen, O. B., Christensen, J. H., Machenhauer, B. and Bozet, M. 1998. Very high resolution regional climate simulations over Scandinavia: present climate. *J. Climate* **11**, 3204–3229.

Christensen, J. H., Machenhauer, B., Jones, R. G., Schär, C., Ruti, P. M. and co-authors 1997. Validation of present-day regional climate simulations over Europe: LAM simulations with observed boundary conditions. *Clim. Dynam.* **13**, 489–506.

Esteban-Parra, M. J., Rodrigo, F. S. and Castro-Diez, Y. 1998. Spatial and temporal patterns of precipitation in Spain for the period 1880–1992. *Int. J. Climatol.* **18**, 1557–1574.

Giorgi, F., Bi, X. and Pal, J. S. 2004. Mean, interannual variability and trends in a regional climate change experiment over Europe. I: Present day climate (1961–1990). *Clim. Dynam.* **22**, 733–756.

Giorgi, F., Bi, X. and Qian, Y. 2002. Direct radiative forcing and regional climatic effects of anthropogenic aerosols over East Asia: a regional coupled climate-chemistry/aerosol model study. *J. Geophys. Res.* **107**, doi:101029/2001JD001066.

Giorgi, F., Bi, X. and Qian, Y. 2003. Indirect vs. direct effects of anthropogenic sulfate on the climate of East Asia as simulated with a regional coupled climate-chemistry/aerosol model. *Climatic Change* **58**, 345–376.

Giorgi, F., Hurrell, J. W., Marinucci, M. R. and Beniston, M. 1997. Elevation signal in surface climate change: a model study. *J. Climate* **10**, 288–296.

Giorgi, F. and Marinucci, M. R. 1996. Improvements in the simulation of the surface climatology of the European region with a nested modeling system. *Geophys. Res. Lett.* **23**, 273–276.

Giorgi, F., Marinucci, M. R. and Bates, G. T. 1993a. Development of a second generation regional climate model (REGCM2). Part I: Boundary layer and radiative transfer processes. *Mon. Weather Rev.* **121**, 2794–2813.

Giorgi, F., Marinucci, M. R., Bates, G. T. and DeCanio, G. 1993b. Development of a second generation regional climate model (REGCM2). Part II: Cumulus cloud and assimilation of lateral boundary conditions. *Mon. Weather Rev.* **121**, 2814–2832.

Giorgi, F. and Mearns, L. O. 1991. Approaches to regional climate change simulation: a review. *Rev. Geophys.* **29**, 191–216.

Giorgi, F. and Mearns, L. O. 1999. Introduction to special section: regional climate modeling revisited. *J. Geophys. Res.* **104**, 6335–6352.

Goodess, C. M. and Jones, P. D. 2002. Links between circulation and changes in the characteristics of Iberian rainfall. *Int. J. Climatol.* **22**, 1593–1615.

Hanssen-Bauer, I. and Førland, E. 2000. Temperature and precipitation variations in Norway 1900–1994 and their links to atmospheric circulation. *Int. J. Climatol.* **20**, 1693–1708.

Hurrell, J. W. 1995. Decadal trends in the North Atlantic Oscillation: regional temperature and precipitation. *Science* **269**, 676–679.

Ion-Bordei, N. 1988. *Meteoclimatic Phenomena Induced by the Carpathian Configuration in the Romanian Plain*. Academiei, Bucharest (in Romanian with abstract in English).

Jacob, D., Andrae, U., Elgered, G., Fortelius, C., Graham, L. P. and co-authors 2001. A comprehensive model intercomparison study investigating the water budget during the BALTEX-PIDCAP period. *Meteorol. Atmos. Phys.* **77**(1–4), 19–43.

Jones, R. G., Murphy, J. M. and Noguer, M. 1995. Simulation of climate change over Europe using a nested regional climate model. I: Assessment of control climate, including sensitivity to location of lateral boundary conditions. *Q. J. R. Meteorol. Soc.* **121**, 1414–1449.

Jones, R. G., Murphy, J. M., Noguer, M. and Keen, M. 1997. Simulation of climate change over Europe using a nested regional climate model. Comparison of driving and regional model responses to a doubling of carbon dioxide. *Q. J. R. Meteorol. Soc.* **123**, 265–292.

Kalnay, E., Kanamitsu, M., Kistler, R., Collins, W., Deaven, D. and co-authors 1996. The NCEP/NCAR 40-year reanalysis project. *Bull. Am. Meteorol. Soc.* **77**, 437–470.

Lamb, P. J. and Pepler, R. A. 1987. North Atlantic Oscillation and an application, *Bull. Am. Meteorol. Soc.* **68**, 1218–1225.

Machenhauer, B., Wildenband, M., Bozet, M., Christensen, J. H., Deque, M. and co-authors 1998. *Validation and Analysis of Regional Present Day Climate and Climate Change Simulations Over Europe*, MPI Report No 275. Max Planck Institute for Meteorology, Hamburg.

Martin-Vide, J. and Gomez, L. 1999. Regionalization of peninsular Spain based on the length of dry spells. *Int. J. Climatol.* **19**, 537–555.

McGregor, J. J. 1997. Regional climate modeling. *Meteorol. Atmos. Phys.* **63**, 105–117.

Muñoz-Díaz, D. and Rodrigo, F. S. 2003. Effects of the North Atlantic Oscillation on the probability for climatic categories of local monthly rainfall in southern Spain. *Int. J. Climatol.* **23**, 381–397.

New, M. G., Hulme, M. and Jones, P. D. 2000. Representing twentieth-century space-time climate variability. Part II: Development of 1901–1996 monthly grids of terrestrial surface climate. *J. Climate* **13**, 2217–2238.

Pal, J. S., Small, E. E. and Eltahir, E. A. B. 2000. Simulation of regional-scale water and energy budgets: representation of subgrid cloud and precipitation processes within RegCM. *J. Geophys. Res.* **105**, 29 579–29 594.

Pope, V. D., Gallani, M. L., Rowntree, P. R. and Stratton, R. A. 2000. The impact of new physical parametrizations in the Hadley Centre climate model—HadAM3. *Clim. Dynam.* **16**, 123–146

Pozo-Vázquez, D., Esteban-Parra, M. J., Rodrigo, F. S. and Castro-Diez, Y. 2001. A study of NAO variability and its possible non-linear influences on European surface temperature. *Clim. Dynam.* **17**, 701–715.

Preisendorfer, R. W. 1988. *Principal Component Analysis in Meteorology and Oceanography*. Elsevier, Amsterdam.

Räisänen, J., Hansson, U., Ullerstig, A., Doscher, R., Graham, L. P. and co-authors 2004. European climate in the late twenty-first century: regional simulations with two driving global models and two forcing scenarios. *Clim. Dynam.* **22**, 13–31.

Räisänen, J. and Joelsson, R. 2001. Changes in averages and extreme precipitation in two regional climate model experiments. *Tellus* **53A**, 547–566.

Räisänen, J., Rummukainen, M. and Ullerstig, A. 2001. Downscaling of greenhouse gas induced climate change in two GCMs with the Rossby Centre regional climate model for northern Europe. *Tellus* **53A**, 168–191.

Rodo, X., Baert, E. and Comin, F. A. 1997. Variations in seasonal rainfall in Southern Europe during the present century: relationships with the North Atlantic Oscillation and the El Ninño–Southern Oscillation. *Clim. Dynam.* **13**, 275–284.

Rodríguez-Puebla, C., Encinas, A.H., Nieto, S. and Garmenia, J. 1998. Spatial and temporal patterns of annual precipitation variability over the Iberian Peninsula. *Int. J. Climatol.* **18**, 299–316.

Rodríguez-Puebla, C., Encinas, A. H. and Sáenz, J. 2001. Winter precipitation over the Iberian peninsula and its relationship to circulation indices. *Hydrol. Earth Syst. Sci.* **5**, 233–244.

Rodwell, M. J., Rowell, D. P. and Folland, C. K. 1999. Oceanic forcing of the wintertime North Atlantic oscillation and European climate. *Nature*, **398**, 320–323.

Rogers, J. C. 1997. North Atlantic storm track variability and its association to the North Atlantic Oscillation and climate variability of northern Europe. *J. Climate* **10**, 1635–1647.

Rotach, M. W., Marinucci, M. R., Wild, M., Tschuck, P., Ohmura, A. and co-author 1997. Nested regional simulation of climate change over the Alps for the scenario of a doubled greenhouse forcing. *Theor. Appl. Climatol.* **57** 209–227.

Sáenz, J., Zubillaga, J. and Rodríguez-Puebla, C. 2001. Interannual variability of winter precipitation in the northern Iberian Peninsula. *Int. J. Climatol.* **21**, 1503–1513.

Schmidli, J., Schmutz, C., Frei, c., Wanner, H. and Schaer, C. 2002. Mesoscale precipitation variability in the region of the European Alps during the 20th century. *Int. J. Climatol.* **22**, 1049–1074.

Sneyers, R. 1990. *On the Statistical Analysis of Series of Observations*. WMO Technical Note 143. World Meteorological Organization, Geneva, 6–15.

Solonosky, V. C., Jones, P. D. and Davies, T. D. 2001. Atmospheric circulation and surface temperature in Europe from the 18th century to 1995. *Int. J. Climatol.* **21**, 63–75.

Tomozeiu, R., Lazzeri, M. and Cacciamani, C. 2002. Precipitation fluctuations during the winter season from 1960 to 1995 over Emilia-Romagna, Italy. *Theor. Appl. Climatol* **72**, 221–229.

Ulbrich, U., Christoph, M., Pinto, J. G. and Corte-Real, J. 1999. Dependence of winter precipitation over Portugal on NAO and baroclinic wave activity. *Int. J. Climatol.* **19**, 379–392.

Uvo, C. B. 2003. Analysis and regionalization of northern European winter precipitation based on its relationship with the North Atlantic oscillation. *Int. J. Climatol.* **23**, 1185–1194.

Van Loon, H. and Rogers, J. C. 1978. The see-saw in winter temperatures between Greenland and Northern Europe. Part I: General description. *Mon. Weather Rev.* **106**, 293–310.

Von Storch, H. 1995. Spatial patterns: EOFs and CCA. In: *Analysis of Climate Variability: Applications of Statistical Techniques* (eds H. von Storch and A. Navarra). Springer, Berlin, 227–258.